



Circular dichroism enhancement in plasmonic nanorod metamaterials

D. VESTLER,¹ I. SHISHKIN,^{2,*} E. A. GURVITZ,³ M. E. NASIR,⁴
A. BEN-MOSHE,¹ A. P. SLOBOZHANYUK,^{3,5} A. V. KRASAVIN,⁴
T. LEVI-BELENKOVA,¹ A. S. SHALIN,³ P. GINZBURG,^{2,3}
G. MARKOVICH,¹ AND A. V. ZAYATS⁴

¹*School of Chemistry, Raymond and Beverly Sackler Faculty of Exact Sciences, Tel Aviv University, Tel Aviv 6997801, Israel*

²*School of Electrical Engineering, Tel Aviv University, Tel Aviv, 6997801, Israel*

³*ITMO University, St. Petersburg 197101, Russia*

⁴*Department of Physics, King's College London, Strand, London WC2R 2LS, UK*

⁵*Nonlinear Physics Center, Research School of Physics and Engineering, Australian National University, Canberra, ACT 0200, Australia*

**ivanshishkin@post.tau.ac.il*

Abstract: Optical activity is a fundamental phenomenon originating from the chiral nature of crystals and molecules. While intrinsic chiroptical responses of ordinary chiral materials to circularly polarized light are relatively weak, they can be enhanced by specially tailored nanostructures. Here, nanorod metamaterials, comprising a dense array of vertically aligned gold nanorods, is shown to provide a significant enhancement of the circular dichroism response of an embedded material. A nanorod composite, acting as an artificial uniaxial crystal, is filled with chiral mercury sulfide nanocrystals embedded in a transparent polymer. The metamaterial, being inherently achiral, enables optical activity enhancement or suppression. Unique properties of inherently achiral structures to tailor optical activities pave a way for flexible characterization of optical activity of molecules and nanocrystal-based compounds.

© 2018 Optical Society of America under the terms of the [OSA Open Access Publishing Agreement](#)

OCIS codes: (160.1585) Chiral media; (160.3918) Metamaterials; (250.5403) Plasmonics.

References and links

1. R. W. W. K. Nakanishi and N. Berova, eds., *Circular Dichroism: Principles and Applications* (Wiley-VCH, 2000).
2. D. K. Gramotnev and S. I. Bozhevolnyi, "Plasmonics beyond the diffraction limit," *Nat. Photon.* **4**, 83–91 (2010).
3. P. Ginzburg, D. Arbel, and M. Orenstein, "Gap plasmon polariton structure for very efficient microscale-to-nanoscale interfacing," *Opt. Lett.* **32**, 3288–3290 (2006).
4. S. Nie and S. R. Emory, "Probing single molecules and single nanoparticles by surface-enhanced Raman scattering," *Science* **275**, 1102–1106 (1996).
5. P. L. Stiles, J. A. Dieringer, N. C. Shah, and R. P. Van Duyne, "Surface-enhanced Raman spectroscopy," *Ann. Rev. Anal. Chem.* **1**, 601–626 (2008).
6. A. B. Zrimsek, A. Henry, and R. P. Van Duyne, "Single molecule surface-enhanced Raman spectroscopy without nanogaps," *J. Phys. Chem. Lett.* **4**, 3206–3210 (2013).
7. Y. Fu, J. Zhang, and J. R. Lakowicz, "Largely enhanced single-molecule fluorescence in plasmonic nanogaps formed by hybrid silver nanostructures," *Langmuir* **29**, 2731–2738 (2013).
8. E. Wertz, B. P. Isaacs, J. D. Flynn, and J. S. Biteen, "Single-molecule super-resolution microscopy reveals how light couples to a plasmonic nanoantenna on the nanometer scale," *Nano Lett.* **15**, 2662–2670 (2015).
9. S. S. Oh and O. Hess, "Chiral metamaterials: enhancement and control of optical activity and circular dichroism," *Nano Converg.* **2**, 24 (2015).
10. M. A. Belkin and G. Shvets, "Experimental demonstration of the microscopic origin of circular dichroism in two-dimensional metamaterials," *Nat. Commun.* **7**, 12045 (2016).
11. A. Guerrero-Martinez, B. Auguie, J. L. Alonso-Gomez, Z. Džolić, S. Gómez-Graña, M. Žinić, M. M. Cid, and L. M. Liz-Marzán, "Intense optical activity from three-dimensional chiral ordering of plasmonic nanoantennas," *Angew. Chemie* **123**, 5613–5617 (2011).
12. E. Hendry, T. Carpy, J. Johnston, M. Popland, R. V. Mikhaylovskiy, A. J. Laphorn, S. M. Kelly, L. D. Barron, N. Gadegaard, and M. Kadodwala, "Ultrasensitive detection and characterization of biomolecules using superchiral

- fields," *Nat. Nanotechnol.* **5**, 783–787 (2010).
13. R. Tullius, A. S. Karimullah, M. Rodier, B. Fitzpatrick, N. Gadegaard, L. D. Barron, V. M. Rotello, G. Cooke, A. Laphorn, and M. Kadodwala, "'Superchiral' spectroscopy: detection of protein higher order hierarchical structure with chiral plasmonic nanostructures," *J. Am. Chem. Soc.* **137**, 8380–8383 (2015).
 14. Y. Tang and A. E. Cohen, "Enhanced enantioselectivity in excitation of chiral molecules by superchiral light," *Science* **332**, 6027 (2011).
 15. D. Melnikau, D. Savateeva, Y. K. Gun, and Y. P. Rakovich, "Strong enhancement of circular dichroism in a hybrid material consisting of J-aggregates and silver nanoparticles," *J. Phys. Chem. C* **117**, 13708–13712 (2013).
 16. I. Lieberman, G. Shemer, T. Fried, E. M. Kosower, and G. Markovich, "Plasmon-resonance-enhanced absorption and circular dichroism," *Angew. Chemie Int. Ed.* **47**, 4855–4857 (2008).
 17. A. O. Govorov, Z. Fan, P. Hernandez, J. M. Slocik, and R. R. Naik, "Theory of circular dichroism of dipole interactions and dielectric effects," *Nano Lett.* **10**, 1374–1382 (2010).
 18. T. J. Davis and D. E. Gómez, "Interaction of localized surface plasmons with chiral molecules," *Phys. Rev. B* **90**, 235424 (2014).
 19. J. Kumar, K. George, L. M. Liz-Marzán, and K. G. Thomas, "Nanoscale chirality in metal and semiconductor nanoparticles," *Chem. Commun.* **52**, 12555–12569 (2016).
 20. M. L. Nesterov, X. Yin, M. Scha, H. Giessen, and T. Weiss, "The role of plasmon-generated near fields for enhanced circular dichroism spectroscopy," *ACS Photonics* **3**, 578–583 (2016).
 21. A. García-Etxarri and J. Dionne, "Surface-enhanced circular dichroism spectroscopy mediated by nonchiral nanoantennas," *Phys. Rev. B* **87**, 235409 (2013).
 22. J. Pedersen, N. A. Mortensen, J. Pedersen, and N. A. Mortensen, "Enhanced circular dichroism via slow light in dispersive structured media," *Appl. Phys. Lett.* **91**, 213501 (2007).
 23. Y. Tang and A. E. Cohen, "Optical chirality and its interaction with matter," *Phys. Rev. Lett.* **104**, 163901 (2010).
 24. L. Novotny and N. van Hulst, "Antennas for light," *Nat. Photonics*, **5**, 83–90 (2011).
 25. P. Ginzburg, "Accelerating spontaneous emission in open resonators," *Ann. Phys.* **508**, 571–579 (2016).
 26. D. G. Baranov, R. S. Savelev, S. V. Li, A. E. Krasnok, and A. Alù, "Modifying magnetic dipole spontaneous emission with nanophotonic structures," *Laser Photon. Rev.* **11**, 1600268 (2017).
 27. P. Ginzburg, D. Roth, M. E. Nasir, P. Segovia, A. V. Krasavin, J. Levitt, L. M. Hirvonen, B. Wells, K. Suhling, D. Richards, V. A. Podolskiy, and A. V. Zayats, "Spontaneous emission in nonlocal materials," *Light: Sci. Appl.* **6**, e16273 (2017).
 28. A. P. Slobozhanyuk, P. Ginzburg, D. A. Powell, I. Iorsh, A. S. Shalin, P. Segovia, A. V. Krasavin, G. A. Wurtz, V. A. Podolskiy, P. A. Belov, and A. V. Zayats, "Purcell effect in hyperbolic metamaterial resonators," *Phys. Rev. B* **92**, 195127 (2015).
 29. A. Ben-Moshe, A. O. Govorov, and G. Markovich, "Enantioselective synthesis of intrinsically chiral mercury sulfide nanocrystals," *Angew. Chem. Int. Ed.* **52**, 1275–1279 (2013).
 30. G. A. Wurtz, R. Pollard, W. Hendren, G. P. Wiederrecht, D. J. Gosztola, V. A. Podolskiy, and A. V. Zayats, "Designed ultrafast optical nonlinearity in a plasmonic nanorod metamaterial enhanced by nonlocality," *Nat. Nanotechnol.* **6**, 107–111 (2011).
 31. P. Ginzburg, F. J. Rodríguez Fortuño, G. A. Wurtz, W. Dickson, A. Murphy, F. Morgan, R. J. Pollard, I. Iorsh, A. Atrashchenko, P. A. Belov, Y. S. Kivshar, A. Nevet, G. Ankonina, M. Orenstein, and A. V. Zayats, "Manipulating polarization of light with ultrathin epsilon-near-zero metamaterials," *Opt. Express* **12**, 14907–14917 (2013).
 32. E. D. Palik, *Handbook of Optical Constants of Solids* (Academic Press, 1985).
 33. P. Ginzburg, A. V. Krasavin, A. N. Poddubny, P. A. Belov, Y. S. Kivshar, and A. V. Zayats, "Self-induced torque in hyperbolic metamaterials," *Phys. Rev. Lett.* **111**, 36804 (2013).
 34. A. A. Bogdanov, A. S. Shalin, and P. Ginzburg, "Optical forces in nanorod metamaterial," *Sci. Rep.* **5**, 15846 (2015).
 35. G. A. Wurtz, W. Dickson, D. O'Connor, R. Atkinson, W. Hendren, P. Evans, R. Pollard, and A. V. Zayats, "Guided plasmonic modes in nanorod assemblies: strong electromagnetic coupling regime," *Opt. Express* **16**, 7460–7470 (2008).
 36. A. García-Etxarri, and J.A. Dionne "Surface-enhanced circular dichroism spectroscopy mediated by nonchiral nanoantennas," *Phys. Rev. B* **87**, 235409 (2013).
 37. M. Schäferling, X. Yin, and H. Giessen "Formation of chiral fields in a symmetric environment," *Opt. Express* **20**, 26326–26336 (2012).
 38. M. Schäferling, D. Dregely, M. Hentschel, H. Giessen "Tailoring enhanced optical chirality: design principles for chiral plasmonic nanostructures," *Phys. Rev. X* **2**, 31010 (2012)
 39. K.-T. Tsai, G. A. Wurtz, J.-Y. Chu, T.-Y. Cheng, H.-H. Wang, A. V. Krasavin, J.-H. He, B. M. Wells, V. A. Podolskiy, J.-K. Wang, Y.-L. Wang, and A. V. Zayats, "Looking into meta-atoms of plasmonic nanowire metamaterial," *Nano Lett.* **14**, 4971–4976 (2014).
 40. B. Wells, A. V. Zayats, and V. A. Podolskiy, "Nonlocal optics of plasmonic nanowire metamaterials," *Phys. Rev. B* **89**, 035111 (2014).
 41. Giovanni Pellegrini, Marco Finazzi, Michele Celebrano, Lamberto Duó, and Paolo Biagioni, "Chiral surface waves for enhanced circular dichroism," *Phys. Rev. B* **95**, 241402(R) (2017)
 42. D. J. Roth, A. V. Krasavin, A. Wade, W. Dickson, A. Murphy, S. Kéna-Cohen, R. Pollard, G. A. Wurtz, D. R. Richards, S. A. Maier, and A. V. Zayats, "Spontaneous emission inside a hyperbolic metamaterial waveguide," *ACS Photonics*

4, 2513–2521 (2017).

43. G. Marino, P. Segovia, A. V. Krasavin, P. Ginzburg, N. Olivier, G. A. Wurtz, and A. V. Zayats, “Second-harmonic generation from hyperbolic plasmonic nanorod metamaterial slab,” *Laser Phot. Rev.* **12**, 1700189 (2018).

1. Introduction

Optical activity in bulk materials manifests itself via different responses to right and left circularly polarized light. Circular dichroism (CD) [1] is a particular yet very important case, where a material has different absorption coefficients for light of opposite handedness. This bulk characteristic reflects inherent topological properties of a matter on microscopic scales. In particular, chirality in molecules originates from absence of mirror symmetry of electronic wavefunctions and corresponding selection rules, resulting in different interactions with left and right circularly polarized light. This inherent physical behavior has major implications in biological functionalities and, as a result, it is frequently used as a sensing parameter for identification and separation of enantiomers in racemic mixtures. Unfortunately, circular dichroism has relatively small optical signature in comparison with dominant linear polarization effects, being 3–4 orders of magnitude smaller than unpolarized absorption in biomolecules [1]. This makes the detection of circular dichroism response from low quantities of analytes even more challenging.

Some of the major efforts in overcoming these challenges are focused on engineering the enhancement of circular dichroism response with nanostructures which enable tailoring and enhancing optical near-fields. From this point of view, plasmonic-based nanostructures enable the field enhancement and confinement on the nanoscale [2, 3] and already led to variety of sensitive spectroscopic techniques, such as surface-enhanced Raman scattering [4–6] and fluorescence [7, 8].

Tailoring a CD response with nanostructured materials follows the same approach. A large number of metamaterials [9, 10] and metamaterial-inspired plasmonic structures [11] demonstrated differential absorption for left- and right-circularly polarized light. Chiral plasmonic structures have been employed for ultrasensitive detection and characterization of biomolecules [12, 13]. CD enhancement has also been demonstrated experimentally with the help of superchiral light [14] and plasmonic nanoparticles [15, 16]. The possibility of CD enhancement by nonchiral structures has been theoretically discussed for intrinsically nonchiral [17–19, 37] and chiral plasmonic nanoparticles [38] and nanoantennas [20], high-permittivity silicon nanoparticles supporting magnetic resonances [21, 36], and dispersive media with slow-light [22].

The use of achiral tailored nanostructures has advantages over chiral nanostructures. For example, the ‘superchiral light’ approach requires tight alignment of optical setups and the enhancement of optical activity is achieved within spatially small regions of space [23]. Sensing enhancement with chiral nanoplasmonic antennas requires very accurate calibration procedures, since inherent optical activity in the nanoantennas themselves dominates the response of tested chiral analytes. Consequently, large-scale achiral substrates, capable of optical activity enhancement, are highly beneficial for a wide range of applications. The basic principle behind this type of enhancement could be qualitatively understood from considering semi-classical description of chiral interactions. Optical activity in molecules originates from simultaneous presence of electric and magnetic dipolar response, whose vectorial components should be as collinear as possible (corresponding matrix element is proportional to the cosine of the angle between electric and magnetic dipoles). Consequently, either electric or magnetic local field enhancements (or even better both simultaneously) could substantially enhance the efficiency of optical rotation.

Various plasmonic structures (antennas) were shown to deliver high electric Purcell enhancements via small modal volumes [24, 25]. Magnetic Purcell factors could be achieved with high-index dielectric particles [21, 26]. However, in the majority of isolated plasmonic antenna-based configurations local field enhancement is achieved in small spatial regions. At the

same time, molecules, being statistically spread within the volume, have decreased probability to experience such enhancement, and, as the result, overall improvement of a signal is relatively low.

On the other hand, large-scale metamaterials, utilizing coupling between adjacent unit cells, can provide high field enhancement over large areas [28]. In particular, arrays of free standing, vertically aligned nanorods have been recently shown to exhibit strong optical anisotropy [31] and deliver record high Purcell enhancement of fluorescence from the emitters located between the rods inside the metamaterial [25]. The basic mechanism behind this type of enhancement is an interplay between local near-field interactions and macroscopically averaged enhancement within the composite [35]. While the far-field optical properties (reflection, absorption, transmission) of such a metamaterial are well described by the effective medium approximation, the internal structure of the local fields is important for considerations of the interaction with molecules placed inside a metamaterial [25]. These local fields are formed by hybridization of the cylindrical surface plasmon modes of the individual nanorods in the array [39,40]. Additionally, waveguided modes of the metamaterial slab of a finite thickness may have strong influence on local density of states [42] and nonlinear effects [43]. Here we demonstrate that the gold nanorod metamaterial can be used as an efficient platform for circular dichroism enhancement. By tailoring the collective response of the nanorods, it is possible to amplify the CD signal of optically active nanocrystals (NCs) by a factor of two.

2. Experimental methods

Metamaterial fabrication. Plasmonic nanorod metamaterials (Figs. 1, 2) were fabricated by Au electrodeposition into highly ordered nanoporous anodic alumina oxide (AAO) templates on glass cover slips [30,31]. An Al film of 700 nm thickness was deposited on a substrate by magnetron sputtering. The substrate comprised a glass cover slip with a 10 nm thick adhesive layer of tantalum pentoxide and a 7 nm thick Au film, acting as a weakly conducting layer. Highly ordered, nanoporous AAO was synthesized by a two step-anodization in 0.3M oxalic acid at 40 V. After an initial anodization process, the formed porous layer was partly removed by etching in a solution of H_3PO_4 (3.5%) and CrO_3 (20 g L^{-1}) at 70°C , which resulted in an ordered pattern. At the next step, the sample was anodized again under the same conditions as in the first step. The anodized AAO was subsequently etched in 30 mM NaOH to achieve pore widening. Gold electrodeposition was performed with a three electrode system, using a non-cyanide solution. Free standing gold nanorod metamaterials were obtained after dissolving the nanoporous alumina template in a mix solution of 0.3 M NaOH and 99.50% ethanol. The length of nanorods was controlled by the electrodeposition time. Small aspect ratio rods were used in order to reduce absorption and avoid artifacts in the CD measurements. Under normal incidence illumination used throughout this work, only one absorption resonance is observed related to plasmonic modes excited with the electric field perpendicular to the nanorod axes [Fig. 1(b)]. The calculated effective permittivity components of the studied metamaterial are presented in Fig. 1(c).

HgS nanocrystals synthesis. Mercury (II) nitrate monohydrate 98.5%, Thioacetamide 98% and Polyvinyl alcohol 99% hydrolyzed (146000-186000 Mw) (PVA) were purchased from Sigma-Aldrich, D-penicillamine 99% was purchased from Fluka, Sodium hydroxide pellets were purchased from Frutarom, and Isopropyl Alcohol AR (IPA) was purchased from Gadot. All materials were used without additional treatment. Deionized water were prepared by an USF Elga UHQ water purifier. Nanocrystal synthesis was performed in disposable receptacles rinsed with deionized water. The process is described in detail in [29]. An aqueous solution of $\text{Hg}(\text{NO}_3)_2 \cdot \text{H}_2\text{O}$ (100 mM, 0.9 mL) was added to 3 mL of deionized water followed by an aqueous solution of D-penicillamine (0.9 mL, 100 mM), an aqueous solution of NaOH (0.3 mL, 1M) and finally an aqueous solution of Thioacetamide (0.9 mL, 100 mM). The solution was vigorously stirred during the addition and allowed to stir for several hours in the dark at room temperature. The product was separated and washed by adding roughly the same volume of IPA to the solution

(the solution turns turbid when shaken once enough has been added) followed by centrifugation (5000 RPM, 5 min) and redispersion in deionized water (this process was repeated 2–3 times).

Metamaterial infiltration. The HgS NCs solution was concentrated via the centrifugation process described above and mixed in a 1:1 volume ratio with 4% w/w PVA aqueous solution so the resulting solution would be 10 times more concentrated than the synthesis product. This NCs-polymer mixture was spin-coated on the gold nanorod samples by depositing 50 μL with the spin-coater (NiLo scientific) set at 3000 RPM for 120 s. The typical size of the HgS NCs is in the range of 10–20 nm.

Circular dichroism measurements. CD measurements were performed with an Applied Photophysics Chirascan CD spectrometer at normal incidence. The substrates were mounted on a sample holder which can rotate around the normal to the substrate and make sure that the CD spectra do not change with rotation, in order to eliminate linear polarization anisotropy artifacts.

Numerical modeling. The finite elements method was used for numerical modeling of the effect. The model of the metamaterial with a nanorod of a radius of 30 nm was considered in non-absorbing dielectric medium with refractive index of 1.5 and thickness of 300 nm. Material parameters of gold nanorods were obtained by linear interpolation of experimentally available data [32]. The dielectric slab with the gold rods was placed on a silica substrate in contact with a perfectly matched layer (PML) in order to emulate an infinitely thick substrate. Periodic boundary conditions were applied to the unit cell, corresponding to the inter-rod distance of 100 nm, in order to replicate an infinite array of nanorods. The chiral medium which fills the space between the rods, was introduced via the following constitutive relations:

$$\begin{aligned}\vec{D} &= \epsilon\vec{E} - ik\sqrt{\epsilon\mu}\vec{H} \\ \vec{B} &= \mu\vec{H} + ik\sqrt{\epsilon\mu}\vec{E},\end{aligned}\quad (1)$$

where \vec{D} , \vec{E} , \vec{B} , and \vec{H} are the electric displacement, electric field, magnetic induction, and magnetic field, respectively. The averaged background permittivity was $\epsilon=2.25$ and $\mu=1$. Both electric and magnetic susceptibilities were assumed to be isotropic. The small size of individual nanocrystals (10-20 nm) compared to the wavelength of light allows to consider PVA-nanoparticle mixture as homogeneous chiral medium embedded in the nanorod array. Dispersion of the Pasteur medium (k) was extracted from the experimental data reported in [29].

3. Results and discussion

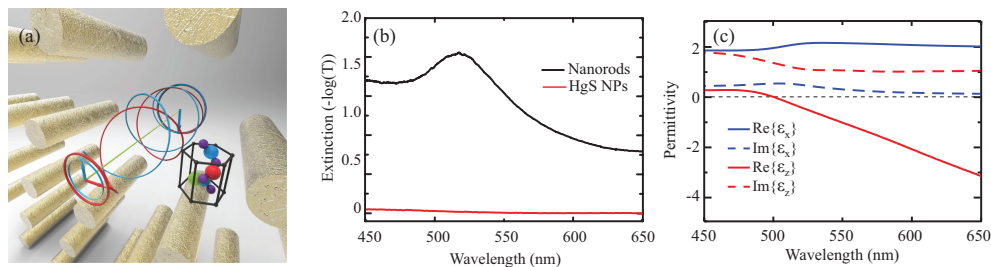


Fig. 1. (a) Schematic of the nanorod metamaterial with a chiral nanocrystal (a hexagonal box) introduced between the nanorods. (b) Normal-incidence extinction spectra measured for the metamaterial (black line) and HgS nanoparticles (red line). The metamaterial parameters are 60 ± 10 nm nanorod diameter, 270 nm length, and 100 ± 20 nm nanorod array period; the nanorods are in air. (c) Effective permittivity components of the nanorod metamaterial calculated using the metamaterial parameters as in (b).

We investigated the chiral response of enantio-pure HgS nanocrystals dispersed in a polymer

film and introduced between the nanorods. It should be noted that the HgS nanocrystals have an intrinsically chiral crystal structure (space group $P3_121$ or $P3_221$). When they are prepared in the presence of chiral L-penicillamine molecules it was shown that primarily one enantiomorph is formed, which exhibits very large CD signal at the absorption threshold of the nanocrystals at ~ 550 nm [29]. This enables overlapping the CD resonance of the NCs with the resonance of the metamaterial at normal illumination [Fig. 1(b)]. In order to demonstrate the enhancement of circular dichroism, the nanorod metamaterial was infiltrated with a 2% polyvinyl alcohol (PVA) aqueous solution containing enantio-pure HgS NCs [Fig. 2]. The contribution of the NCs to overall extinction of the composite is negligible compared to the extinction of the metamaterial alone [Fig. 1(b)].

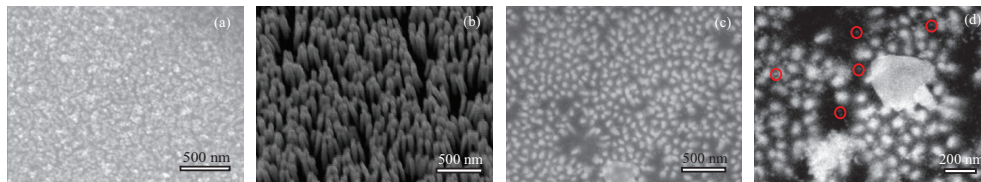


Fig. 2. SEM images of (a) HgS nanocrystals drop-casted on silicon substrate, (b) nanorod metamaterial before spin-coating the PVA layer with HgS NCs, (c) metamaterial after the PVA coating with HgS NCs, (d) Zoomed view of (c). Red circles mark the positions of individual HgS NCs.

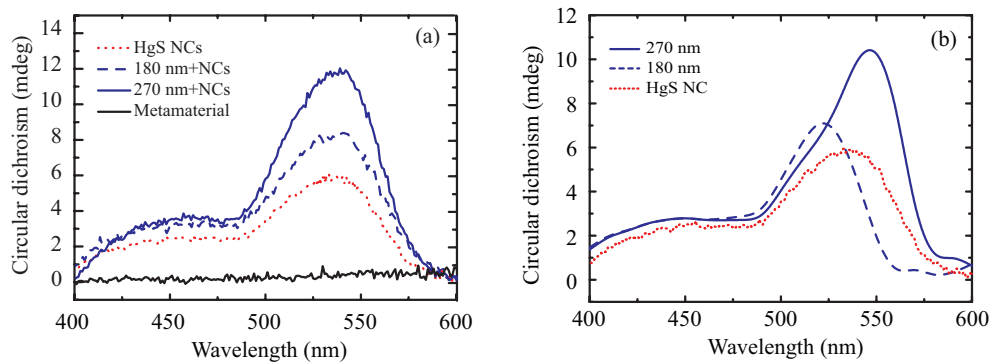


Fig. 3. (a) Experimental circular dichroism spectra of the HgS NCs in a PVA film on a glass substrate (red line), the metamaterial before (black line) and after (blue lines) coating with the PVA-HgS NCs film for the nanorod lengths of 180 nm (dashed blue line) and 270 nm (solid blue line). (b) Numerically calculated circular dichroism of the HgS NCs (red line) and the metamaterial-HgS NCs composite for the nanorod length of 180 nm (dashed blue line) and 270 nm (solid blue line). All other parameters of the metamaterials are as in Fig. 1 (b). Both experiments and simulations are performed at normal incidence.

The CD spectrum of the bare nanorods (before coating) shows a weak non-zero CD signal [Fig. 3(a)] which can be attributed to minor tilts of individual rods from the normal to the sample surface, resulting in minor anisotropy of absorption of LCP and RCP light by the samples. On the other hand, CD of HgS NCs embedded in the PVA film on a glass substrate (without the metamaterial) has a pronounced resonance around 525 nm and a wide shoulder at shorter wavelengths. The metamaterial clearly influences the CD of the nanocrystals and the enhancement depends on the nanorod length. The maximum observed enhancement is about two-fold in the case of the longest rods (280 nm). It is important to note that the CD signal, defined as a difference

between transmission coefficients of right and left circularly polarized light, normalized by their sum, does not depend on the thickness of a film under investigation.

The repeatability of the observed enhancement was verified in a set of control experiments. The PVA layer with HgS NCs was washed away with a mixture of deionized water, IPA and dimethylsulphoxide heated to 70°C followed by the CD spectroscopy of the washed sample. Afterwards, a new coating of PVA-HgS NCs was deposited on the cleaned nanorod array followed by CD spectroscopy. The sample was then coated with PVA without HgS NCs in order to check, that no optical activity was introduced by PVA coating. The small changes (< 25% in the enhancement factor) between repeated coating cycles are believed to be due to slightly different polymer distribution on the sample surface achieved at each cycle and minor differences in the positioning of the sample in the experimental set-up.

In order to understand the impact of the metamaterial on the CD enhancement, the propagation of circularly polarized waves in the metamaterial with chiral NCs was numerically studied. The modelled CD response for both the PVA-NCs film on a glass substrate is in good correspondence with the experimental spectra [Fig. 3(b)]. In the case of the metamaterial composite, a very good agreement with the experiment in terms of the enhancement factor and the spectral response is obtained for 270 nm long rods, without any additional fitting parameters. At the same time, for shorter rods (180 nm length), while the same trend is observed as in the experiment, the overall spectral shape is somewhat different (this may be attributed to uncertainties in geometrical parameters of the nanorod arrays and the thickness of the polymer layer, spin coated within the free standing rods template). It is worth noting the alternative approach for determining the CD

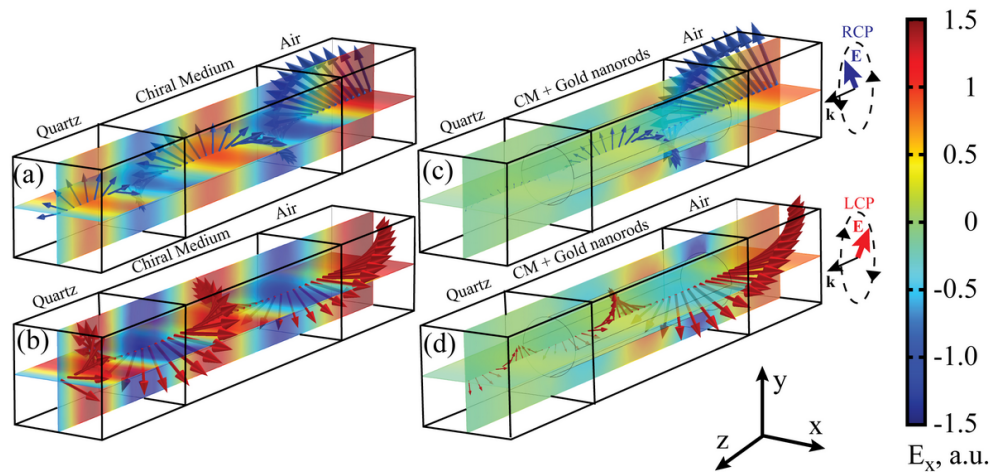


Fig. 4. Simulated electromagnetic wave propagation (from right to left) through (a,b) chiral medium without the metamaterial and (c,d) chiral medium embedded in the metamaterial for (a,c) LCP and (b,d) RCP incident light. The instantaneous field E_x is shown as a color map. Arrows indicate the direction of the electric field with their length being proportional to the instantaneous field amplitude (panels (a,b)) and its logarithm (panels (c,d)). For the visualization purposes the chiral parameter k was increased 1,000 times compared to the experimental value.

enhancement, which relies on the evaluation of the chiral fields of the nanostructures [36–38]. To estimate a collective response from an anisotropic composite such as a nanorod metamaterial infiltrated with chiral molecules, the chiral field within the auxiliary structure (a nanorod array

without molecules) should be integrated over a volume which it occupies. CD enhancement comes from the geometry of the structure and, in the first approximation, does not depend on the chiral molecules themselves. Remarkably, while isolated dipolar resonators do not provide an overall chiral enhancement [37], the nanorod metamaterial case provides conceptually different scenario because of a formation of a collective mode of a composite due to the near-field coupling between the nanorods. As the result, the nanorod metamaterial, being achiral itself, exhibits peculiar properties of the collective CD enhancement. This effect is similar to the recently theoretically predicted CD enhancement due to molecular coupling to achiral nanoparticles [15] and in planar multilayers, which can be considered as another example of the metamaterial with strong coupling between adjacent plasmonic structures, similar to the metamaterial studied here [41].

The electric field distribution and its orientation simulated for right (RCP) and left (LCP) circularly polarized waves propagating through the metamaterial with and without chiral NCs are shown in Fig.4. Panels (a) and (b) demonstrate the case of a bulk chiral material without an auxiliary nanostructure. For the visualization purposes, the chirality parameters were artificially increased by three orders of magnitude with respect to the experimentally obtained data, in order to facilitate visual comparison between the amplitudes of RCP and LCP waves propagating through thin material layer. One can see that a RCP wave (blue arrows) experience larger absorption in the medium. Introduction of the nanorod metamaterial significantly increases linear propagation losses [Fig. 4(c and d)]. Nevertheless, the discrimination between RCP and LCP (ratio between the amplitudes of the transmitted waves) becomes larger in comparison to the case of a chiral medium alone. This visual example allows to observe the impact of the auxiliary plasmonic structure on the CD properties.

4. Conclusions

We have shown that the nanorod metamaterial can be used for CD enhancement of chiral molecules placed between the nanorods. When the metamaterial resonance was tuned to spectrally overlap with the chiroptical resonance of the NCs, an overall two-fold CD enhancement was observed. The near-field interaction between the HgS NCs and the nanorods forming the metamaterial dictates the overall chiral behavior. Several light-matter interaction processes tailored by the nanorod metamaterials were previously investigated and the local field effects, similar to those responsible for the CD enhancement, were shown to be an important factor in determining optical properties of molecules and nano-objects placed inside a metamaterial, which can not be described in a conventional effective medium approximation [33, 34]. Collective macroscopic enhancement of microscopic optical activity with large scale self-assembled nanostructures is of paramount importance for enabling many applications, where accurate optical sensing of circular dichroism is required.

Funding

EPSRC (UK); ERC iPLASMM (321268); TAU Rector grant; PAZY foundation; German-Israeli Foundation (2399); Israel Science Foundation (507/14); Russian Foundation for Basic Research (16-52-00112); Russian Science Foundation (16-12-10287); Ministry of Education and Science of Russian Federation (SP-4248.2016.1, 3.4982.2017/6.7); Royal Society; Wolfson Foundation.